Proc. Natl. Acad. Sci. USA
Vol. 90, pp. 10250–10254, November 1993
Biophysics

Relationship between NMR transverse relaxation, trabecular bone architecture, and strength

(magnetic susceptibility/trabecular structure/bone strength/lumbar vertebrae)

H. CHUNG†, F. W. WEHRLI†‡, J. L. WILLIAMS§, AND S. D. KUGELMASS†¶

Departments of †Radiology and §Orthopedic Surgery, University of Pennsylvania Medical Center, Philadelphia, PA 19104

Communicated by John D. Roberts, July 6, 1993

ABSTRACT **Structure, biomechanical competence, and incremental NMR line broadening (R_2') of water in the intertrabecular spaces of cancellous bone were examined on 22 cylindrical specimens from the lumbar vertebral bodies of 16 human subjects 24–86 years old (mean, 60 years old). A strong association ($r = 0.91$; $P < 0.0001$) was found between Young's modulus of elasticity and R_2' for a wide range of values corresponding to cancellous bone of very different morphologic composition. NMR line broadening is caused by the inhomogeneity of the magnetic field induced as a consequence of the coexistence of two adjacent phases of different diamagnetic susceptibility—i.e., mineralized bone and water in the marrow spaces. Structural analyses performed by means of NMR microscopy and digital image processing indicated that the variation in R_2' is closely related to the trabecular microstructure. Mean trabecular plate density measured along the direction of the magnetic field was found to play a major role in predicting R_2' ($r = 0.74$; $P < 0.0001$). This behavior was confirmed when the plate density was varied in individual specimens, which was achieved by rotating the specimen, making use of the bone's structural anisotropy. It is concluded that the NMR transverse relaxation rate in human cancellous bone of the spine is significantly determined by trabecular structural parameters relevant to biomechanical strength. The results further underscore the important role played by the transverse trabeculae in contributing to cancellous bone strength. The work has implications on possible *in vivo* use of quantitative magnetic resonance for the assessment of fracture risk in osteoporotic patients.**

It is widely accepted that the mechanical strength of the skeleton in vertebrates is largely determined by the material density of trabecular bone, generally referred to as bone mineral density (BMD). Osteopenia, characterized by a loss in bone mass, leads to impaired bone strength, which, in turn, has been associated with atraumatic vertebral fractures suffered by patients with osteoporosis (1). The association between bone strength and BMD has been suggested by a large number of studies, with bone strength statistically showing a quadratic dependence on density (2). However, *in vivo* BMD measurements by either quantitative computed tomography or dual-energy x-ray absorptiometry do not very well predict fracture risk in osteoporotic patients (3).

More recently, the search for a better predictor of bone strength, and thus fracture risk, has shifted toward trabecular bone morphology (4–8). Kleerekoper (5) found in a study in which postmenopausal women with vertebral fractures were compared to age-matched normal women of equal mean BMD that osteoporotics had significantly lower trabecular plate density and, as a corollary, higher trabecular plate thickness. The data were interpreted as suggesting that an equivalent amount of trabecular bone distributed as widely spaced, disconnected, thick trabeculae, is biomechanically less competent than numerous connected thin plates.

In 1991 Wehrli *et al.* (9) reported preliminary clinical results with a quantitative NMR technique developed by them. The method is based on the measurement of the intrinsic magnetic field inhomogeneity caused by the different magnetic permeability of mineralized bone and the protons in water and triacylglycerides of hematopoietic and fatty marrow in the intertrabecular spaces. Specifically, they measured T_2^*, the effective transverse relaxation time, showing that in patients with osteoporosis T_2^* was significantly prolonged, which was postulated to arise from increased intertrabecular spacing. Support for this interpretation was provided in an additional study in which it was shown that in regions of known denser trabeculation, such as the epiphysis of the distal femur, T_2^* was shorter than in the metaphysis and diaphysis (10). Similar results were also provided by Majumdar *et al.* (11) *in vitro* in cadaver specimens of human vertebral bodies where a positive correlation was found between quantitative computed tomography BMD and $1/T_2^*$. A more recent study reported an analogous relationship *in vivo* in the distal radius and femur ($r = 0.85$; $P < 0.0001$ in the radius) (12). Clearly, if the T_2^* measurement merely duplicated the result of bone densitometry, the method would be of questionable value. However, a recent theoretical analysis of model lattices of cancellous bone indicates that the width of the magnetic field histogram, which determines T_2^*, critically depends on the geometry and orientation of the lattice elements (13).

The first objective of the present work was to explore the theoretically predicted relationship between the magnetic field distribution in cancellous bone from human lumbar vertebrae and architectural parameters such as intertrabecular spacing and thickness, as well as the orientation of the trabeculae with respect to the polarizing field. The second objective was to confirm the hypothesis that T_2^* is an indicator of trabecular strength by measuring Young's modulus of elasticity in the same specimens in which the microstructure was evaluated.

THEORY

Decay Rate of the Transient NMR Signal. The rate of decay ($1/T_2^*$) of the transient NMR signal is determined by interactions among the nuclear dipoles, as well as interactions between the latter with the polarizing field. Nonuniformity of the magnetic field results in a distribution of resonance frequencies and thus additional dephasing of the spin isochromats‖ that make up the transverse magnetization, thus

The publication costs of this article were defrayed in part by page charge payment. This article must therefore be hereby marked "*advertisement*" in accordance with 18 U.S.C. §1734 solely to indicate this fact.

Abbreviations: BMD, bone mineral density; T_2^*, effective transverse relaxation time; TE, echo time.

‡To whom reprint requests should be addressed.
¶Present address: Department of Computer and Information Science, New Jersey Institute of Technology, Newark, NJ 07102.

‖A spin isochromat refers to the magnetization of an infinitesimally small volume element within which the field can be regarded as uniform.

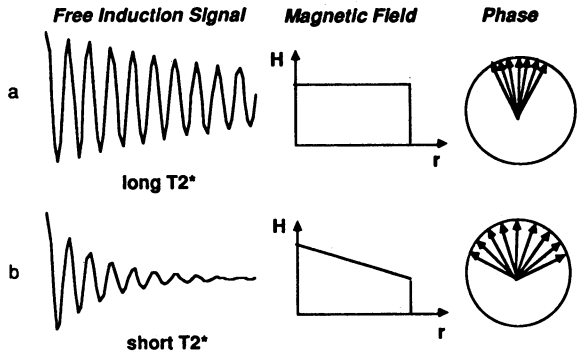

FIG. 1. Effect of magnetic field inhomogeneity on T_2^*. (*a*) Homogeneous field. (*b*) Inhomogeneous field. Note that the more inhomogeneous the field along some spatial coordinate *r*, the faster the isochromats constituting the magnetization are dephased and thus the shorter the time constant is for signal decay (T_2^*).

leading to a further damping of the FID—i.e., shortening of T_2^*. Hence, a homogeneous magnetic field (Fig. 1*a*) is consistent with long T_2^*, whereas an inhomogeneous field (Fig. 1*b*) leads to a progressive shortening of T_2^*. In the present case, we make use of intrinsic magnetic field inhomogeneities caused by the makeup of the tissue—i.e., trabecular bone and bone marrow.

Effect of Discontinuous Magnetic Susceptibility. It is well known that the polarizing magnetic field causes a magnetic surface potential at the phase boundary of two materials of different magnetic susceptibility. Mineralized bone, by virtue of the higher atomic number of its elemental composition (i.e., calcium and phosphorus), is more diamagnetic than marrow constituents in the trabecular marrow cavities, which consist mainly of water and lipids (i.e., oxygen, carbon, and hydrogen). This tiny difference in susceptibility is sufficient to cause a spatially varying magnetic field in the intertrabecular space, which is responsible for the shortening of the T_2^* of trabecular bone marrow.

Consider two adjoining materials of susceptibility χ_m and χ_b. The induced surface charge density σ at the interface between the two materials then is

$$\sigma = \Delta\chi \mathbf{H}_o \cdot \mathbf{n}, \qquad [1]$$

where $\mathbf{n}$ is the unit vector normal to the interface and $\Delta\chi = \chi_m - \chi_b$. The additional field resulting from the magnetic charges at the phase boundary is given by (14)

$$\mathbf{H}_i(\mathbf{r}) = \int dS' \left(\frac{\sigma(\mathbf{r} - \mathbf{r}')}{|\mathbf{r} - \mathbf{r}'|^3} \right), \qquad [2]$$

with integration running over the surface of the interface, and $\mathbf{r} - \mathbf{r}'$ being the vector from the source to the field point (Fig. 2). Therefore, the induced field is proportional to the difference in susceptibility of the two adjoining materials, the strength of the applied field, and the inverse square of the distance between source and field location. For an array of trabeculae, the field is thus expected to be highly inhomogeneous and we postulate that a relationship exists between the magnetic field distribution within the volume of interest, and the number density, thickness, and orientation of trabeculae.

For the subsequent discussion it is convenient to adopt the following definitions:

$$1/T_2' \equiv R_2' \approx \frac{\gamma \Delta H_{iz}}{2}, \qquad [3]$$

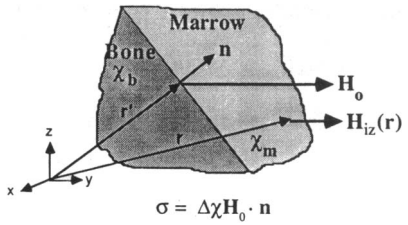

FIG. 2. Diamagnetic material is polarized by magnetic field $\mathbf{H}_o$ leading to surface charge densities $\Delta\chi\mathbf{H}_o\cdot\mathbf{n}$ at the phase boundary and a spatially varying magnetic field $\mathbf{H}_i(\mathbf{r})$, whose *z* component gives rise to the line broadening of bone marrow protons.

where ΔH_{iz} is the full width at half maximum of the magnetic field histogram in the volume of interest such as an imaging voxel. R_2' thus is the contribution to the effective transverse relaxation rate, $1/T_2^*$, arising from local magnetic field inhomogeneity

$$1/T_2^* = 1/T_2 + R_2'. \qquad [4]$$

MATERIALS AND METHODS

Sample Preparation. Twenty-two human lumbar spine specimens from L3–L5 were harvested at autopsy from 16 recently deceased human subjects (24–86 years old; mean, 60 years old), with the specimens kept frozen until used. Cylindrical cores, parallel to the spinal axis, were drilled from the vertebral bodies with a diamond coring bit of 1.3 cm (inner diameter) and cut to a length of 1.3 cm on a Buehler Isomet low-speed saw to obtain flat and parallel end faces suited for mechanical testing. After nondestructive testing, the bone marrow was removed by immersing the bone specimens in hypochlorite for 1 day and was rinsed repeatedly with hot water. Subsequently, the samples were suspended in distilled water for the measurement of T_2^* at 1.5 T. The rationale for marrow removal is 2-fold: (*i*) Upon removing the cortex and coring the bone, contact with oxygen leads to a transformation of hemoglobin in hematopoietic marrow from the diamagnetic oxy to the paramagnetic deoxy state. The cellular confinement of paramagnetic deoxyhemoglobin leads to intrinsic gradients, which cause considerable further shortening of the effective transverse relaxation time (15). (*ii*) Cutting the intact bone causes fluid to leak out. The resulting air cavities are detrimental to both NMR microscopy and T_2^* measurements in that they lead to local field distortions caused by the difference in susceptibility between air and marrow tissue. It is to be noted that these effects are not present *in vivo*.

Measurement of Young's Modulus. The samples were mechanically tested at room temperature in compression between two smooth compression platens at a strain rate of 0.001 s^{-1} with a 2.5 N preload until a maximum strain of ≈0.5%. The test was repeated twice. The specimens were kept moist with saline throughout the test. Displacement was measured by a linear variable differential transformer (LVDT between the two platens). The force and displacement were recorded on an $x - y$ recorder. Strains were then calculated by using the original dimensions of the cylinder as measured with a micrometer. Young's modulus was determined from the steepest portion of the load − displacement curve.

Measurement of Intrinsic Magnetic Field Inhomogeneity. The drilled defatted cores were placed in cylindrical glass vials of ≈1.4 cm (inner diameter) filled with distilled water from which the NMR signal was derived. Experiments to measure T_2^* were performed on a 1.5 T magnetic resonance scanner (General Electric Signa). For this purpose, the vials were oriented such that the axes of the cylindrical specimens were parallel to the main magnetic field H_o. To minimize

global magnetic field inhomogeneity arising from the finite length of the vials, the assembly of vials was immersed in water so as to match the susceptibility inside to the one outside the vials.

T_2^* was measured by fitting signal amplitudes collected as a function of echo time (TE) within a 1.3 × 1.3 cm^2 region of interest in coronal images to a decaying exponential (Fig. 3). The image voxel size was 1 × 2 × 5 mm^3, and data corresponding to 12 TE values were collected. T_2 was measured by means of a single-slice Hahn spin-echo sequence, using seven TE values ranging from 50 to 500 ms. Subsequently, R_2' was computed from T_2^* and T_2 for each specimen by means of Eq. 4. Reproducibility was evaluated for eight samples, each measured three times, affording a SD of 0.35–1.47 s^{-1}.

NMR Microscopy and Image Analysis. Two-dimensional proton NMR microscopic imaging on these specimens was performed on a Bruker AM-400 9.4 T wide-bore spectrometer/microimaging system. Specimens were placed with their cylindrical axes collinear with the direction of the magnetic field. For each specimen, three or four slices were acquired both transaxially and longitudinally. The terms transaxial and longitudinal refer to an image plane perpendicular and parallel to the specimen's cylindrical axis, respectively. Typical voxel sizes were on the order of 30 × 30 × 150 μm^3.

Micromorphometric parameters were obtained by subjecting the images to an automated image analysis program developed in the authors' laboratory. Images at various processing stages and the pixel intensity histogram are shown in Fig. 4. The original images were first converted to binary format prior to analysis. At the resolution chosen (≈30 μm relative to the average trabecular thickness of 50–250 μm in the human lumbar vertebrae) and a signal-to-noise ratio of 15–20, classification of the pixels into bone and water in the marrow space was straightforward. For this purpose, an intensity threshold was selected on the pixel intensity histogram at the midpoint between the two peaks corresponding to bone and water. Under the resolution conditions chosen, segmentation is insensitive to the precise threshold (cf. Fig. 4*e*). Pixels having lower intensity than the threshold value were assigned to bone; those of higher intensity were assigned to marrow space. Single pixels of anomalously high or low intensity were attributed to noise and eliminated by means of a median filter applied to the binary image (16).

Bone area fraction was obtained by pixel counting within the region of interest. The total bone perimeter was estimated by creating a smoothed polygon following detection of the boundary pixels. Mean trabecular plate thickness, d_m, was computed as the bone area divided by one-half the perimeter (17). Mean intercept length, l_m (i.e., the mean separation between trabeculae), was measured by drawing parallel test lines, spaced 130 μm apart, at the desired angle and averaging the length of the lines within marrow spaces (Fig. 5). Mean trabecular plate density, ρ_m, was then calculated as $1/(d_m + l_m)$. Because of the directional dependence of magnetic charge polarization, as discussed earlier, we need the component of ρ_m along the direction of the static field, $\rho_{m(s/i)}$, which is the inferior–superior direction of the spine.

RESULTS

Fig. 6 shows the relationship between Young's modulus of elasticity measured in human lumbar vertebrae, plotted as a function of R_2', indicating a linear correlation with a slope of ≈19.9 MPa/s^{-1} ($r = 0.91$; $P < 0.0001$). This important result proves that there is a strong positive correlation between trabecular bone strength and the bandwidth of the induced

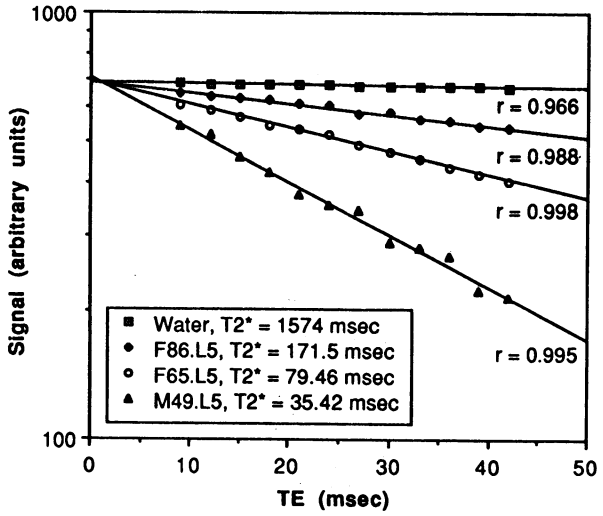

FIG. 3. Amplitude of gradient-echo signal S(TE) plotted versus TE. Solid lines are best fits to $S(TE) = S_0 \exp(-TE/T_2^*)$, indicating that, within the range of TE values chosen, the assumption of exponential decay is valid. Note the significantly different decay time constants for trabecular bone from different subjects (diamonds = female, 86 years old; circles = female, 65 years old; triangle = male, 49 years old).

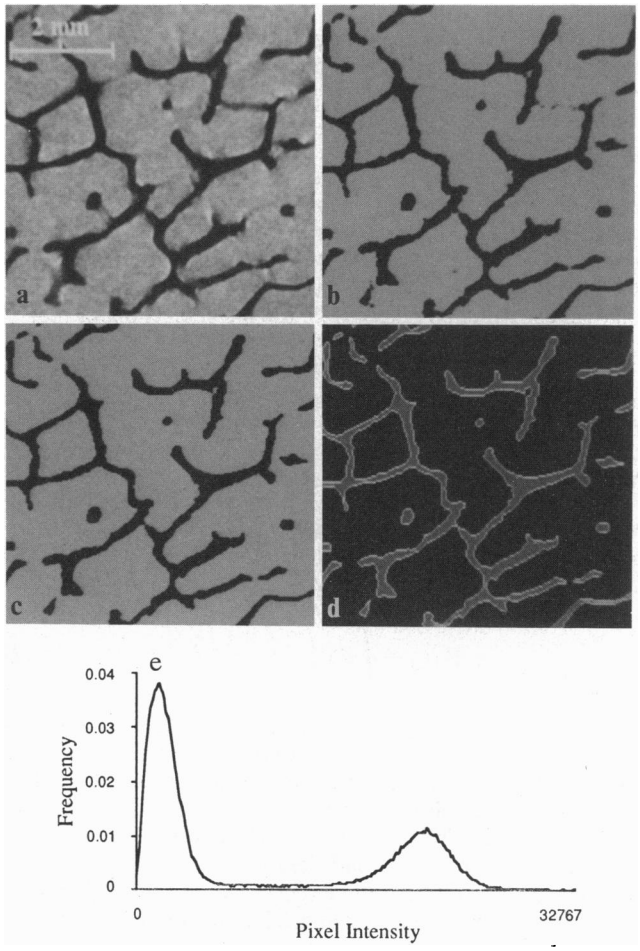

FIG. 4. (*a–d*) 400-MHz transaxial NMR images of trabecular structure from L5 lumbar vertebra (male, 61 years old) at various stages of processing. (*a*) Raw image. (*b*) Segmented binary image. (*c*) Binary image following application of median filter for the removal of isolated pixels. (*d*) Image showing boundary pixels highlighted. (*e*) Pixel intensity histogram displaying two well separated peaks pertaining to bone and background (left) and intertrabecular space assignable to bone marrow (right).

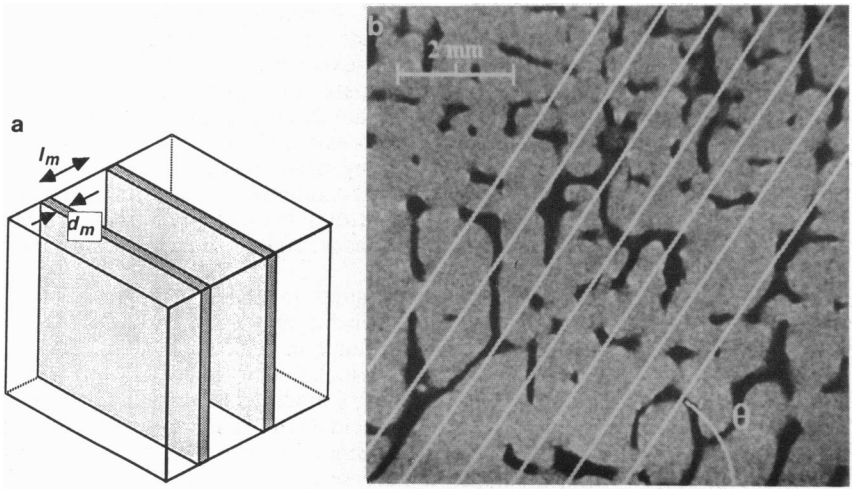

FIG. 5. (*a*) Schematic drawing showing trabecular plates of thickness d_m and spacing l_m. Trabecular plate density $\rho_m = (l_m + d_m)^{-1}$ is defined as the mean number of trabecular plates per unit length along some direction. (*b*) Longitudinal NMR image of the L4 lumbar vertebra (male, 49 years old), showing parallel test lines used to measure l_m, the mean distance between trabeculae.

magnetic field. Although Young's modulus is not equivalent with ultimate strength, there is a strong association between the two parameters (18, 19). We note that the linearity between stiffness and R_2' is valid over a wide range of values corresponding to cancellous bone of very different morphologic composition. The most significant conclusion to be drawn is that a global measurement of R_2' in cancellous bone seems able to predict the stiffness of this complicated structure with high accuracy.

The second question concerns the causes of the variation in R_2', in terms of the bone's microstructure. In Fig. 7 R_2' is plotted versus $\rho_{m(s/i)}$, showing a positive correlation ($r = 0.74$; $P < 0.0001$). This correlation is somewhat weaker than the one between Young's modulus and R_2', suggesting R_2' to be dominated by more than one structural parameter. A closer inspection of two specimens of very similar trabecular plate density but very different R_2' (labeled F51 and M61 in Fig. 7) sheds some light on this question. We find that the specimen with anomalously low R_2' (F51) also had very low mean trabecular thickness (99 μm, compared to 127 ± 21 μm in 22 specimens). We postulate that both decreased trabecular thickness and increased intertrabecular spacing should result in increased magnetic field homogeneity and thus decreased R_2' for which the correlation between R_2' and d_m lends some support ($r = 0.63$; $P < 0.02$; data not shown).

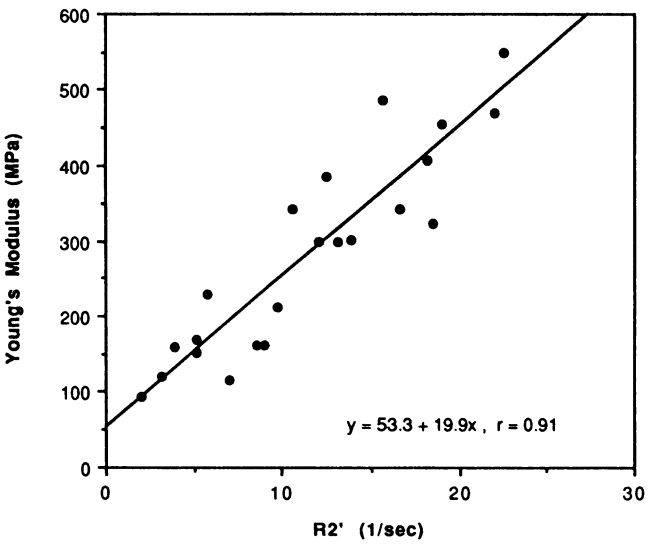

FIG. 6. Young's modulus of elasticity obtained from compression of human lumbar vertebrae in inferior–superior direction, plotted as a function of R_2', the contribution to the effective transverse relaxation rate of the water protons in the intertrabecular spaces.

It has recently been shown in models of trabecular bone that the distribution of the magnetic field variation (to which R_2' is proportional) scales approximately linearly with both number density of the structural elements as well as their thickness (13). Clearly, variation of any one of these geometric parameters can also affect BMD. Therefore, the empirically established association between R_2' and BMD, measured by quantitative computed tomography (12), is not too surprising. The latter finding was confirmed by our data, except that bone fraction, derived from the analysis of the NMR images, was used in lieu of BMD. The data afforded a positive correlation ($r = 0.78$; $P < 0.0001$), analogous to the association between R_2' and ρ_m.

We argue from a mechanistic point of view that variations in BMD *per se* cannot explain variations in R_2'. To prove this hypothesis, an experiment was conceived that keeps BMD constant while varying plate density along the field direction. The experiment exploits the anisotropic nature of trabecular bone in that plate density has a directional dependence. For this purpose, a cylindrical core was drilled from a lumbar vertebral body with the axis of symmetry collinear with the anterior–posterior direction, and the vial holding the bone specimen was oriented perpendicular to the direction of the static magnetic field $\mathbf{H_o}$. Subsequently, the vial was rotated

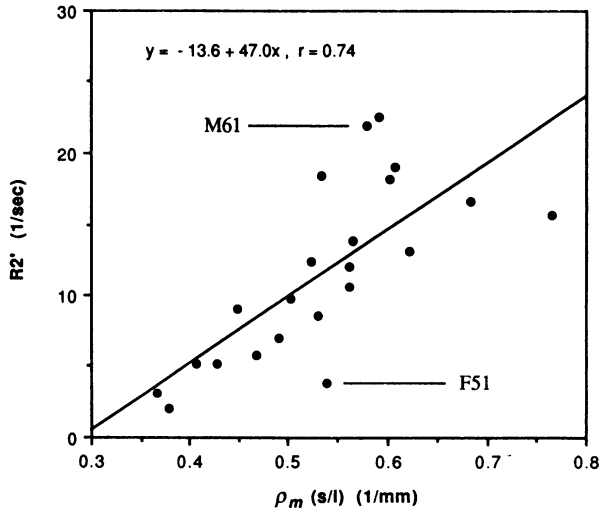

FIG. 7. R_2' versus mean trabecular plate density $\rho_{m(s/i)}$, indicating increased line broadening with increasing $\rho_{m(s/i)}$, in accordance with the hypothesis. The two outlying data points corresponding to comparable ρ_m (L4, male 61 years old; L5, female 51 years old) were characterized by particularly large (M61) and small (F51) plate thickness.

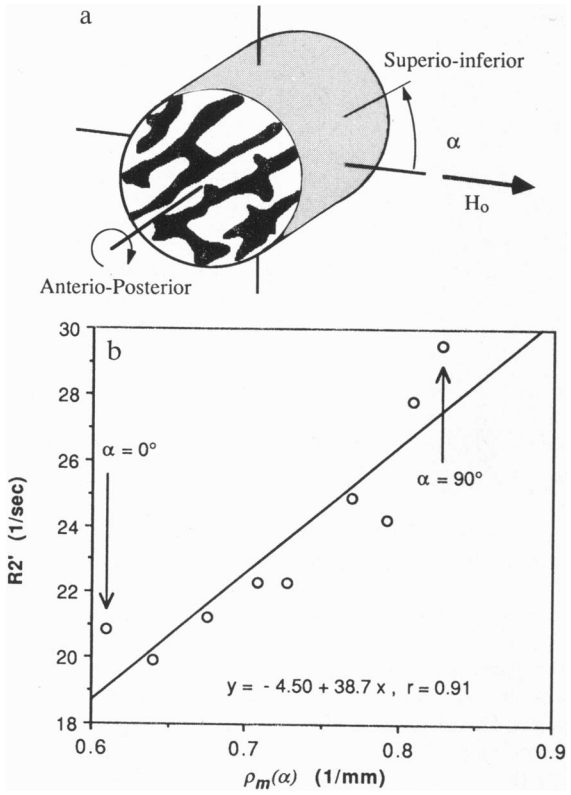

FIG. 8. (*a*) Experimental arrangement for measuring R_2' for different plate densities $\rho_m(\alpha)$, with α being the angle between the magnetic field and the anatomic inferior–superior direction. (*b*) R_2' versus $\rho_m(\alpha)$ measured in vertebral body specimens from a typical subject, showing R_2' to increase from $\alpha = 0°$ to $\alpha = 90°$.

around the cylindrical specimen axis in 10° increments from $\alpha = 0°$ to 90° (Fig. 8*a*), with α being the angle between the direction of $\mathbf{H_o}$ and the superior–inferior direction of the bone specimen and R_2' measured at each angle. Any variation in R_2' is unrelated to BMD and is likely to arise from a variation in plate density, ρ_m, which was measured for each angle on the basis of the transaxial NMR images. Fig. 8*b* shows the resulting association between R_2' and ρ_m in a typical specimen. The positive correlation between the density of trabecular plates orthogonal to the field and R_2' provides strong evidence in support of our hypothesis that increased plate density causes line broadening. Experimental results from six other specimens showed similar positive correlation of R_2' with ρ_m in the direction of the applied field, although slopes and intercepts varied (between ≈30 and 120 s^{-1}/mm^{-1} for the slope). The correlation coefficient was 0.9 or greater in all cases. The differences observed among specimens imply that other structural parameters play a role in determining the absolute value of R_2'.

DISCUSSION AND CONCLUSION

In this work, we have corroborated the theoretically predicted relationship between R_2', expressing the extent of local magnetic field inhomogeneity and intertrabecular spacing (13) in the same bone specimens for which Young's modulus has been measured in that we have shown R_2' to decrease with increased intertrabecular spacing. Additional strong support for this interpretation has been provided by an experiment in which BMD remains invariant, which was achieved by making use of the angular dependence of the trabecular plate density by virtue of the bone's structural anisotropy. We have shown with this experiment that a highly significant positive correlation exists between R_2' and trabecular plate density in spite of the fact that in this case BMD is unaltered. This finding has been predicted in a model lattice of diamagnetic material mimicking cancellous bone where it was demonstrated that increased number density achieved at the expense of reduced strut thickness (i.e., holding material density constant) increases magnetic field inhomogeneity and thus R_2' (13).

An ongoing patient study involving osteoporotic subjects indicates that a relationship may exist between T_2^* and the biomechanical competence of trabecular bone in the vertebrae (20). The strong association revealed in the present work between R_2' and Young's modulus for uniaxial compressive loading in cadaver specimens of human vertebrae confirms the above hypothesis. Since R_2' is shown to be sensitive to the density of the transverse (i.e., horizontal) trabeculae, the relationship shown in Fig. 6 underscores the critical role the transverse trabeculae play in determining vertebral body strength (8).

Clearly, *in vitro* R_2' or *in vivo* T_2^* ought not be regarded as an absolute predictor of strength. As we have shown, R_2' was found to be greater in the medial–lateral ($\alpha = 90°$) than in the superior–inferior ($\alpha = 0°$) direction, contrary to the behavior for maximum stress, which is 2–3 times smaller in the transverse than in the longitudinal direction (21). Thus, only if other variables, such as the anatomic location or the orientation relative to the applied field are held constant, R_2' (or T_2^*) can be used as a strength predictor.

This work was supported by National Institutes of Health Grant RO1 AR40671-01A1.

1. Melton, L. J., Chao, E. Y. S. & Lane, J. (1988) in *Osteoporosis: Etiology, Diagnosis, and Management*, eds. Riggs, B. L. & Melton, L. J. (Raven, New York), pp. 111–131.
2. Gibson, L. J. (1985) *J. Biomech.* **18**, 317–328.
3. Heuck, A. S., Block, J., Glueer, C., Steiger, P. & Genant, H. K. (1989) *J Bone Miner. Res.* **4**, 891–900.
4. Parfitt, A. M., Mathews, C. H. E., Villanueva, A. R., Kleerekoper, M., Frame, B. & Rao, D. S. (1983) *J. Clin. Invest.* **72**, 1396–1409.
5. Kleerekoper, M., Villanueva, A. R., Stanciu, J., Rao, D. S. & Parfitt, A. M. (1985) *Calcif. Tissue Int.* **37**, 594–597.
6. Weinstein, R. S. & Hutson, W. S. (1987) *Bone* **8**, 137–142.
7. Hodgskinson, R. & Currey, J. D. (1990) *Proc. Inst. Mech. Eng.* **204**, 115–121.
8. Mosekilde, L. (1989) *Bone* **10**, 425–432.
9. Wehrli, F. W., Ford, J. C., Attie, M., Kressel, H. Y. & Kaplan, F. S. (1991) *Radiology* **179**, 615–621.
10. Ford, J. C. & Wehrli, F. W. (1991) *Magn. Reson. Med.* **17**, 543–551.
11. Majumdar, S., Thomasson, D., Shimakawa, A. & Genant, H. K. (1991) *Magn. Reson. Med.* **22**, 111–127.
12. Majumdar, S. & Genant, H. K. (1992) *J. Magn. Reson. Imaging* **2**, 209–219.
13. Ford, J. C., Wehrli, F. W. & Chung, H. (1993) *Magn. Reson. Med.* **30**, 373–379.
14. Morrish, A. (1983) *The Physical Principles of Magnetism* (Krieger, Malabar, FL).
15. Ford, J. C., Wehrli, F. W., Williams, J. L. & Wehrli, S. L. (1991) *J. Magn. Reson. Imaging* **1**, 193.
16. Jain, A. K. (1989) *Fundamentals of Digital Image Processing* (Prentice Hall, Englewood Cliffs, NJ).
17. Gundersen, H. J. G., Bendtsen, T. F., Korbo, L., Marcussen, N., Moller, A., Nielsen, K., Nyengaard, J. R., Pakkenberg, B., Sorensen, F. B., Vesterby, A. & West, M. J. (1988) *Acta Pathol. Microbiol. Immunol. Scand.* **96**, 379–394.
18. Goldstein, S. A. (1987) *J. Biomech.* **20**, 1055–1061.
19. Rice, J., Cowin, S. & Bowman, J. (1988) *J. Biomech.* **21**, 155–168.
20. Wehrli, F. W., Ford, J. C., Haddad, J. G., Kaplan, F. S. & Attie, M. (1993) *J. Magn. Reson. Imaging* **3**, 59.
21. Mosekilde, L., Vidik, A. & Mosekilde, L. (1985) *Bone* **6**, 291–295.